

## Thermalization slowing down of weakly nonintegrable quantum spin dynamics

Budhaditya Bhattacharjee <sup>1,\*</sup>, Alexei Andreanov <sup>1,2,†</sup> and Sergej Flach <sup>1,2,‡</sup>

<sup>1</sup>Center for Theoretical Physics of Complex Systems, *Institute for Basic Science (IBS)*, Daejeon 34126, Republic of Korea

<sup>2</sup>Basic Science Program, *Korea University of Science and Technology (UST)*, Daejeon 34113, Republic of Korea



(Received 22 May 2024; revised 21 December 2024; accepted 25 March 2025; published 14 May 2025)

We study thermalization slowing down of a quantum many-body spin system upon approach to two distinct integrability limits. Motivated by previous studies of classical systems, we identify two thermalization timescales: one quantum Lyapunov timescale is extracted by quantifying operator growth in time on an appropriately defined basis, while another ergodization timescale is related to the statistics of fluctuations of the time-evolved operator around its mean value based on the eigenstate thermalization hypothesis. Using a paradigmatic quantum Ising chain, we find that both timescales diverge upon approach to integrability. We investigate the relative strength of the divergence in the two limits and find that, despite significant qualitative differences in the mechanism of integrability breaking, the timescales diverge in a similar fashion. This allows us to establish a universality of integrability breaking in quantum spin dynamics.

DOI: [10.1103/PhysRevResearch.7.023149](https://doi.org/10.1103/PhysRevResearch.7.023149)

### I. INTRODUCTION

The study of integrable and chaotic dynamics in quantum systems is an area of active investigation with the goal of explaining the emergence of statistical mechanics in interacting quantum systems, among others. Multiple observables have been identified and studied as probes of integrable/chaotic dynamics. One class of such probes is based on spectral properties of the system [1–8] rooted in the Bohigas-Giannoni-Schmit (BGS) and Berry-Tabor conjectures [1,2] and the expected random matrixlike behavior of quantum systems [9,10]. Another class of observables is based on the operator growth or state evolution under integrable/chaotic Hamiltonians. Observables such as out-of-time-ordered correlation (OTOC) functions [11–23], circuit complexity [24–27], operator size [28–31], and Krylov complexity [32–39] fall into this category.

Thermalization is a closely related phenomenon to the study of chaos. It describes late-time physics at equilibrium and leads to the emergence of statistical mechanics. Thermalization is a universal property of nonintegrable systems, found in both classical and quantum dynamics. Specifically, we are interested in the nature of thermalization near integrability, where it is expected to slow down. This has been explored extensively in classical systems. Some of the key features studied in this respect are the relevant timescales: Lyapunov

time, ergodization time, etc. These timescales are obtained by computing different observables and studying their divergence upon approach to integrability [40–49].

In quantum mechanical systems, the eigenstate thermalization hypothesis (ETH) [50–56] is often used to characterize thermalization. Within the purview of ETH, there are ergodization timescales (e.g., Thouless time) [52,57–60] which have been explored in various systems. These timescales differ between chaotic and integrable systems, and their exact nature has been studied extensively. Another active direction of investigation involves the notion of Lyapunov-like timescales for quantum systems. Operator growth serves as a potential path (via OTOCs) to define an appropriate spectrum [61–63]. Similarly, the spectral function is also used [64]. In quantum systems without well-defined classical limits (e.g., spin- $\frac{1}{2}$  chains) the quantum Lyapunov spectra behave quite differently from classical spectra and may suffer from definition ambiguities [62,63]. There are better-defined notions of the *maximum Lyapunov exponent*, which is typically extracted from the growth exponent of an appropriately defined observable. These include the exponent of the OTOC [65] and Krylov complexity [32,37].

In this paper, we extend the concept of timescales, originally developed for classical networks, to quantum mechanical systems near integrability. We introduce the notion of quantum networks near integrability and characterize them by studying the dynamics of conserved quantities of the limiting integrable Hamiltonian. We employ the operator growth approach (using Krylov complexity) to define an appropriate notion of Lyapunov time. Operator growth is captured through the lens of Krylov complexity, which describes the evolution of an operator on a minimal basis. We then use ETH principles to extract another timescale, which we coin the *ergodization timescale* (in analogy to classical systems). The system that we study is a prototypical one-dimensional (1D) quantum Ising spin- $\frac{1}{2}$  chain. Near the integrable limits, the two

\*Contact author: budhadityab@ibs.re.kr

†Contact author: aalexei@ibs.re.kr

‡Contact author: sflach@ibs.re.kr

timescales are compared. Their behavior is used to identify universal features of integrability breaking, by considering qualitatively different mechanisms of integrability breaking, which we call short-range network (SRN) and long-range network (LRN) by analogy with the classical case [40–47].

## II. THE MODEL

The prototypical spin system we employ to characterize LRNs and SRNs is the quantum Ising chain (QIC) [66,67] given by the following Hamiltonian:

$$H = - \sum_{i=1}^N (J\sigma_i^z \sigma_{i+1}^z + g\sigma_i^z + h\sigma_i^x), \quad (1)$$

where  $J$ ,  $g$ , and  $h$  are real numbers describing nearest-neighbor interaction and longitudinal and transverse magnetic fields, respectively. The  $\sigma_i^{x,z}$ 's are Pauli matrices, describing spin- $\frac{1}{2}$  algebra. The system is, in general, nonintegrable and has been extensively studied through various probes of quantum chaos [68–73]. In the limits  $g \rightarrow 0$  [transverse field Ising model (TFIM)] or  $h \rightarrow 0$  [longitudinal field Ising model (LFIM)], the Hamiltonian in Eq. (1) becomes integrable. We study chaos and thermalization timescales in the vicinity of these limits to observe and quantify the possible differences between the two limits.

In classical systems near integrable limits, the way the actions are coupled by the integrability-breaking perturbations defines different classes of networks with different properties. The system is defined as a LRN if the connectivity (defined through an appropriately defined *coupling range*) is extensive in the number of actions  $N$ . In a SRN, the connectivity of the actions (i.e., the coupling range) is independent of the number of actions.

Inspired by the classical definition, we focus on the conserved quantities of the QIC in its integrable limits. In the limit  $h = 0$ , the spin chain becomes effectively decoupled in real space, and the conserved quantities are local, with the simplest one being  $\sigma_i^z$ . Adding a small nonzero value of  $h$  will couple these conserved quantities in a local manner of a SRN.

In the limit  $g = 0$ , the spin chain is extensively connected while still being integrable. This is reflected by the fact that the conserved quantities are nonlocal [74]. Some of these operators correspond to simple symmetry operations. For example, the spin-flip operation  $\sigma^z \rightarrow -\sigma^z$  for all spins leaves the Hamiltonian invariant. The corresponding conserved quantity is  $\prod_{i=1}^N \sigma_i^x$ . Other conserved quantities are similarly represented as extensive (nonlocal) combinations of the local spin matrices or as sums of local terms. The support of such quantities grows with system size [75].

Thus, by analogy with the classical definition [45–47], we classify the quantum weakly nonintegrable models by the character of coupling of conserved quantities in the integrable limit by the integrability breaking perturbation. We consider the following two types of networks: (i) *Quantum SRN*—a conserved quantity in the integrable limit is coupled by the integrability-breaking perturbation to a system size-independent number of other conserved quantities, as observed from the operator dynamics defined by standard commutator relations. (ii) *Quantum LRN*—a

conserved quantity in the integrable limit is coupled by the integrability-breaking perturbation to a number of other conserved quantities that scale with the system size.

In what follows, we probe the ergodicity (ETH) and operator growth timescales of the above operators near the two respective limits. We then compare the divergence of these two timescales upon approaching each of the two limits.

## III. KRYLOV COMPLEXITY

There exists a large class of observables that quantify operator growth under Hamiltonian dynamics. A common feature among most of these probes is the choice of a basis to expand the time-evolved operator. Once the basis is chosen, then appropriate *expectation values* are defined and evaluated, which then serve to distinguish between chaotic and integrable systems.

One such probe is Krylov complexity [32]. The steps to evaluate Krylov complexity begin with generating a minimal basis [76], which is called the *Krylov basis*. The Krylov complexity captures the average position of an operator in a minimal basis under the unitary evolution in time of the operator with the Hamiltonian  $H$ . The construction of the Krylov basis relies on an appropriately chosen norm in the Hilbert space of operators. We employ the infinite-temperature Hilbert-Schmidt norm for our analysis

$$\langle A|B \rangle = \frac{\text{Tr}(A^\dagger B)}{\mathcal{D}}. \quad (2)$$

Upon adopting the norm, one chooses an operator  $\mathcal{O}$  whose evolution is studied. The unitary evolution of  $\mathcal{O}$  governed by the Hamiltonian  $H$  is defined as

$$\mathcal{O}(t) = e^{iHt} \mathcal{O} e^{-iHt} = e^{i\mathcal{L}t} \mathcal{O}, \quad (3)$$

where  $\mathcal{L}(\ast) \equiv [H, \ast]$  is the Liouvillian superoperator. The elements  $\mathcal{O}_n$  of the minimal (Krylov) basis corresponding to the operator  $\mathcal{O}$  and Hamiltonian  $H$  are generated via the Lanczos algorithm [32,77], as described in Appendix A. The operator  $\mathcal{O}(t)$  has the following expansion in this basis:

$$\mathcal{O}(t) = \sum_n i^n \psi_n(t) \mathcal{O}_n. \quad (4)$$

The dynamical properties of  $\mathcal{O}(t)$  under the Hamiltonian  $H$  are encoded in the behavior of the Krylov wave functions  $\psi_n(t)$ . These properties allow us to diagnose chaotic behavior in quantum many-body systems [32,34–38].

It was argued in Ref. [32] that the average position of the time-evolved operator

$$K(t) = \sum_n^{\mathcal{K}} n |\psi_n(t)|^2, \quad (5)$$

known as Krylov complexity, grows exponentially with  $t$  for chaotic dynamics:  $K(t) \sim e^{2\alpha t}$ . The exponent  $\alpha$  captures the strength of the chaotic dynamics and is bounded from above by the Maldacena-Shenker-Stanford [65] bound. One can then define a natural timescale for a chaotic system as  $\alpha^{-1}$ , which we denote as  $T_\lambda$  throughout this paper since it captures the growth of operators under the Hamiltonian  $H$ .

#### IV. ERGODIZATION TIME

The ETH [50,54] provides a powerful tool to study and characterize thermalization in quantum mechanical systems. It serves as a way to probe the chaotic or integrable dynamics of a system through the evolution of operators and states. The essential statement of ETH can be encapsulated in the following equation:

$$\langle \mathcal{O}(t) \rangle|_{t \rightarrow \infty} = \bar{\mathcal{O}} + \frac{1}{\sqrt{\mathcal{D}}} R(t), \quad (6)$$

where the expectation value  $\langle \dots \rangle$  of the time-evolved operator is taken in a typical state, and the long time-averaged expectation value of the operator  $\bar{\mathcal{O}}$  can be evaluated analytically in the diagonal ensemble. The function  $R(t)$  represents subleading fluctuations, suppressed by the Hilbert space dimension  $\mathcal{D}$ . The nature of the function  $R(t)$  has been studied extensively in different chaotic and integrable systems [78–81]. We use the fluctuations of  $R(t)$  to extract a timescale that we refer to as the ergodization timescale  $T_E$ . The definition of this scale largely follows that in the classical case, discussed in Ref. [40]. We choose a random initial state  $|\psi\rangle$  as the typical state and track the evolution of  $\mathcal{O}(t)$ . As the function  $\langle \mathcal{O}(t) \rangle$  evolves, it eventually starts to fluctuate around the mean value  $\bar{\mathcal{O}}$ , going above and below the mean with time. This defines the passage times  $t_i$  of the function across the mean value  $\langle \mathcal{O}(t_i) \rangle = \bar{\mathcal{O}}$  [40–47]. Time intervals between the two subsequent passages

$$\tau_i = t_{i+1} - t_i \quad (7)$$

are called excursion times since they reflect the time spent by the expectation value  $\langle \mathcal{O}(t) \rangle$  away from its mean value. We distinguish additionally positive  $\tau_{i,+}$  and negative  $\tau_{i,-}$  excursion times for excursions above and below the mean value  $\bar{\mathcal{O}}$ . For a given system and operator, the collected excursion times  $\tau_i$  obey some distribution. We use the moments—mean and variance—of this distribution to extract an ergodization timescale, as defined later and discussed in the Appendix D.

#### V. RESULTS

We study numerically the dynamical properties close to integrability of the quantum SRNs and LRNs, respectively, using the definitions and the methods outlined above. The Hamiltonian is given by Eq. (1), and we choose the following conserved quantities in the two integrable limits of the Hamiltonian as the time-evolved operators/observables whose dynamical properties we study:

$$\mathcal{O}_{h \rightarrow 0} = \sigma_i^z, \quad (8)$$

$$\mathcal{O}_{g \rightarrow 0}^{(k)} = I^{(k)}, \quad k = 1, \dots, N, \quad (9)$$

where  $I^{(k)}$  denotes the set of conserved quantities for the TFIM

$$I^{(k)} = iJ \sum_{j=1}^N (S_{j:j+k}^{zy} - S_{j:j+k}^{yz}), \quad (10)$$

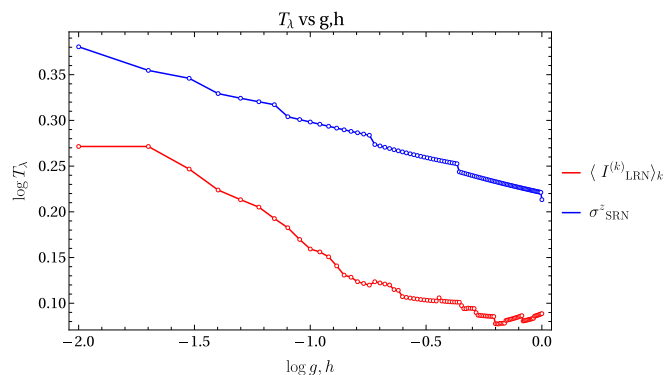


FIG. 1. Lyapunov time  $T_\lambda$  for  $N = 8$  spins extracted from the linear growth of the Lanczos coefficients of time-evolved operator  $\mathcal{O}(t)$  in the Krylov basis as a function of  $h$  for short-range network (SRN) and  $g$  for long-range network (LRN; averaged), respectively. In both limits,  $T_\lambda$  shows a clear increase upon approach to the integrable limit.

where we have the following shorthand

$$S_{j:j+l}^{\alpha\beta} = \sigma_j^\alpha \left( \prod_{n=1}^{l-1} \sigma_{j+n}^x \right) \sigma_{j+l}^\beta. \quad (11)$$

The conserved quantity  $\mathcal{O}_{h \rightarrow 0}^{(k)}$  comprises sums of  $q$ -local quantities, which have support on  $q$  lattice sites. For  $I^{(k)}$ , we have  $q = k + 1$ . At the respective integrable limits, the operators are conserved, their corresponding Lyapunov exponents are 0, and their Lyapunov times are defined through the Krylov complexity diverge. Like the classical case, we are interested in quantifying the divergence of the Lyapunov and ergodization times (from the two probes) upon approaching the integrable limits. For the following discussion, we will present the timescales obtained by averaging over the  $N$  operators  $\mathcal{O}_{g \rightarrow 0}^{(k)}$  in the LRN case. The individual timescales are presented in Appendix C. For the SRN case, averaging over the  $N$  possible  $\sigma_i^z$  gives quantitatively similar timescales to that of an individual  $\sigma_i^z$ . This is discussed in the Appendix B.

Figure 1 shows the Lyapunov times  $T_\lambda$  extracted from the linear growth of the Lanczos coefficients in the Krylov basis of the operators in Eqs. (8) and (9) and plotted in the log-log scale as functions of the integrability breaking parameters  $g$  (LRN) or  $h$  (SRN). Our LRN data for  $T_\lambda$  are in semiquantitative agreement with similar computations in Ref. [32], although the Hamiltonian parameters do not completely match, and different operators were used.

In both LRN and SRN cases, the observed behavior of  $T_\lambda$  is fitted with a (weak) power-law divergence for small values of  $g$  or  $h$ . One may consider other fitting attempts for different model families in Ref. [32], which involve logarithmic fits. The differences are small in the considered parameter range, and all that matters for our purpose here is to use the same fitting procedure for all measured timescales. The exponents are extracted for a system of  $N = 8$  spins via a linear fit of the

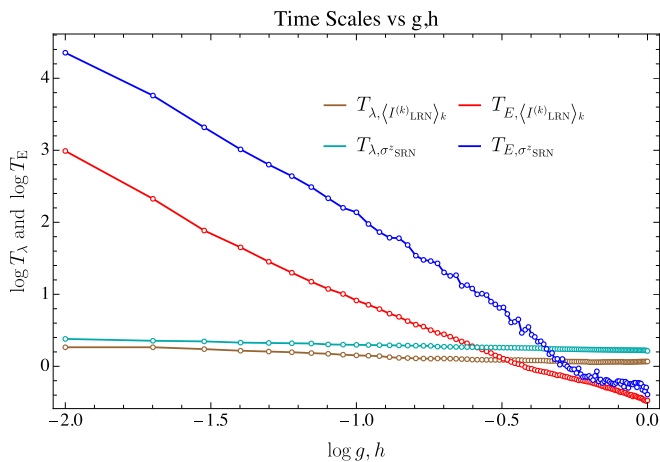


FIG. 2. Comparison of the ergodization time  $T_E$  and Lyapunov time  $T_\lambda$  for the short-range network (SRN; near-Ising limit) and long-range network (LRN; near-Free limit).

data on the log-log scale

$$\log_{10} T_{\lambda, \text{SRN}} = -0.083 \log_{10}(h) + 0.218, \quad (12)$$

$$\log_{10} T_{\lambda, \text{LRN}} = -0.155 \log_{10}(g) + 0.010. \quad (13)$$

To study the thermalization properties, we collect the statistics of the excursion times  $\tau_\pm$  in Eq. (7) of the expectation value of the respective operators in Eqs. (8) and (9) (denoted by the subscripts  $\sigma_{\text{SRN}}^z$  and  $\langle I_{\text{LRN}}^{(k)} \rangle_k$  in the numerical plots) in a random state (different choices of the state yielded similar results). We average the timescales over the  $N$  conserved quantities  $I^{(k)}$  for the LRN case. The results for individual quantities  $I^{(k)}$  in Eq. (10) are discussed in the Appendix C. We study the mean  $\mu$  and variance  $\sigma^2$  of the positive and negative excursion times in Eq. (7). To define an appropriate ergodization time  $T_E$ , we study the relative behavior of mean  $\mu$  and variance  $\sigma^2$ , with the integrability-breaking parameter, by collecting  $10^4$  excursions. Increasing this number does not change the moments significantly. The following behavior of the moments is observed, which follows rather closely the classical weakly nonintegrable systems: We observe that the values of  $\sigma$  are exponentially larger than  $\mu$  close to the integrable limit for both SRN and LRN, suggesting that the typical timescale of fluctuations is dominated by the distribution tail rather than its mean. A natural ergodization timescale is then defined as  $T_E = \sigma^2/\mu$  [40–47].

In Fig. 2, we compare the ergodization times  $T_{E, \pm}$  for the SRN and LRN based on positive/negative excursion times with the Lyapunov time  $T_\lambda$  obtained via the Krylov method. Like the Lyapunov time  $T_\lambda$ , the ergodization time  $T_E$  also shows a power-law divergence with the decrease of the integrability-breaking parameter. The linear fits of the data in the log-log scale are

$$\log_{10} T_{E, \text{SRN}} = -2.263 \log_{10}(h) - 0.137, \quad (14)$$

$$\log_{10} T_{E, \text{LRN}} = -2.073 \log_{10}(g) - 1.150. \quad (15)$$

Ergodization times extracted from positive and negative excursion times  $\tau_\pm$  show similar scaling close to integrability. Here, we discuss the result obtained from  $\tau_+$ .

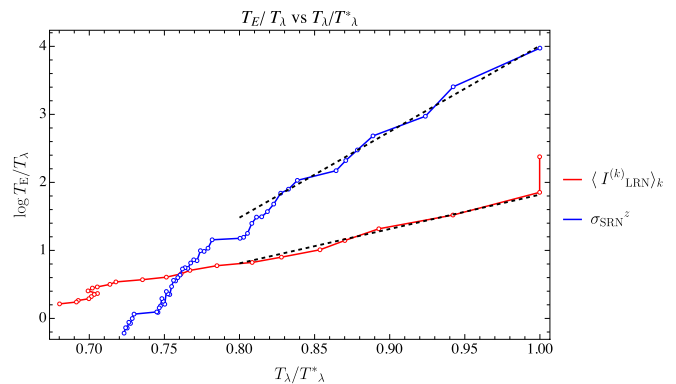


FIG. 3.  $T_E/T_\lambda$  for long-range network (LRN) and short-range network (SRN), plotted with respect to  $T_\lambda/T_\lambda^*$ . The dashed lines represent the linear fit in the log-linear scale. The slopes correspond to  $\alpha = 6.16$  for LRN (in red) and  $\alpha = 12.63$  for SRN (in blue).

Our findings indicate that, in the two integrable limits, the timescales  $T_\lambda$  and  $T_E$  diverge with exponents that differ by at least an order of magnitude. This follows from comparing Eq. (12) with Eq. (14) and Eq. (13) with Eq. (15). Therefore, the timescale associated with ETH diverges exponentially faster than that associated with operator growth. For the two network classes, the Lyapunov and Ergodization timescales, respectively, diverge with comparable exponents. This suggests a universality in the mechanism of integrability breaking in quantum many-body spin systems. The SRN, characterized by local conserved quantities in the integrable limit, demonstrates a slowing down of thermalization at a rate which appears to be like the LRN, which is characterized by nonlocal conserved quantities (which appear as sums of local terms) in the integrable limit. However, such a conclusion can be partially deceiving since we vary different parameters  $g$  and  $h$ . To properly compare the timescales from both network regimes, we replot them in units of the corresponding largest Lyapunov times. This is done in Fig. 3, which is our central result and shows the ratio  $T_{E, \pm}/T_\lambda$  as a function of  $T_\lambda/T_\lambda^*$ . Now we put the timescale analysis of both classes on a similar footing [82]. Here,  $T_\lambda^*$  is the maximum value of  $T_\lambda$  for each (SRN, LRN) of the networks and is required for effective comparison of the two networks since the range of  $T_\lambda$  observed in Fig. 1 is different for the SRN and LRN. It is evident from Fig. 3 that, for the two network classes,  $T_{E, \pm}/T_\lambda$  scales in qualitatively different ways as  $T_\lambda^\alpha$  with  $\alpha \gg 1$ , especially near  $T_\lambda/T_\lambda^* = 1$ . We find a rather weak scaling  $\alpha = 6.16$  for the LRN as compared with a much stronger scaling  $\alpha = 12.63$  for the SRN.

## VI. CONCLUSIONS

In this paper, we investigated the universality classes of thermalization of classical weakly nonintegrable systems in the case of weakly nonintegrable quantum many-body spin systems. The classes are defined by the two timescales quantifying thermalization: One timescale comes from the Krylov complexity of operator growth. In the nonintegrable regime, the K-complexity grows as  $\exp(t/T_\lambda)$ , defining a Lyapunov timescale.

Another timescale, the ergodization time  $T_E$ , is inspired by ETH and is defined through the statistics of the time intervals between consecutive crossings of the expectation of time-evolved operator  $\langle \mathcal{O}(t) \rangle$  around its mean value  $\bar{\mathcal{O}}$ . Here,  $T_E$  is then defined through the appropriate moments of the intervals.

For  $\mathcal{O}$  conserved in the integrable limit, both timescales are expected to diverge.

The SRN is defined by the locality of interaction between the conserved quantities (in the integrable limit) as integrability is weakly broken. We find that the distribution of the crossing intervals is fat-tailed in this case, and therefore,  $T_E$  is defined as the ratio of the variance and the mean.

Conversely, the LRN is defined by the nonlocality of interaction between the conserved quantities upon weak integrability breaking. Like the classical observation [45], we find that the two timescales respond in a qualitatively different way as compared with the SRN case, underscoring the difference of the integrability-breaking mechanisms.

In the 1D spin- $\frac{1}{2}$  chain we study, both timescales,  $T_\lambda$  and  $T_E$ , diverge as power laws with a decreasing integrability-breaking parameter. We compare the exponents of both  $T_E$  and  $T_\lambda$  in the two network classes. We find that the exponents of  $T_E$  and  $T_\lambda$  are comparable with each other for LRN and SRN. However, this result uses varying different model parameters. To quantitatively compare the relative growth of the timescales for both regimes, we measure  $T_E$  in units of  $T_\lambda$  and plot the outcome as a function of  $T_\lambda$ . We then find that the LRN regime shows a relatively small rate at which thermalization (in the ETH sense) slows down upon approaching the integrable limit compared with operator spreading. For the SRN case instead, the rate at which thermalization (in the ETH sense) slows down upon approaching the integrable limit compared with operator spreading is much larger. Therefore, in the SRN case, it takes more and more time to thermalize as compared with the operator growth timescales.

This implies that, in the SRN regime, ETH-like thermalization slows down exponentially faster than operator spreading as integrability is approached.

We identify this drastic difference in the relative slowdown of thermalization, and operator spreading as the universal feature of SRNs, as opposed to LRNs. This is like the character of thermalization slowing down in classical systems [40,41], where classical Lyapunov time is compared with classical ergodization time, and the two network classes respond in very different manners.

Many open questions naturally emerge from this investigation. One natural direction is testing this classification for other types of quantum systems. Further, other probes might be able to distinguish and be sensitive to these two network classes. In the classical case, the Lyapunov spectrum scaling close to integrability proved to be instrumental in classifying network classes [41]. It would be interesting to study probes that do not have classical analogs, such as quantum entanglement [83], in such phenomena. Our investigation was restricted to finite system sizes; the scaling of the two timescales with system size (and therefore in the thermodynamic limit) is also worth investigating. There has also been a large body of work in which authors have investigated the exact nature of the fluctuations of operator evolution [e.g.,  $R(t)$  in Eq. (6)]. This suggests that a more concrete

connection between ETH and ergodization time might exist. Random matrix theory is also expected to play a crucial role in this characterization. It would also be interesting to study the effective random matrix theory near integrability for the two network classes.

## ACKNOWLEDGMENTS

The authors acknowledge Tilen Cadez, Barbara Dietz, Yeongjun Kim, Gabriel Lando, Aniket Patra, Sonu Verma, and Weihua Zhang for relevant discussions. We acknowledge the financial support from the Institute for Basic Science (IBS) in the Republic of Korea through Project No. IBS-R024-D1.

## APPENDIX A: KRYLOV COMPLEXITY

The Krylov complexity of an operator  $\mathcal{O}$  under the effect of the Hamiltonian  $H$  is computed with the following algorithm [32], which generates a basis in the space of operators:

- (1) First element of the basis:  $\mathcal{O}_0 = \mathcal{O}$ .
- (2) Evaluate the commutator of the operator with the Hamiltonian  $\mathcal{A}_1 = [H, \mathcal{O}_0]$ . Note that this is orthogonal to  $\mathcal{O}_0$ .
- (3) Normalize this operator  $\mathcal{O}_1 = \frac{1}{b_1} \mathcal{A}_1$  with  $b_1 = \sqrt{\langle \mathcal{A}_1 | \mathcal{A}_1 \rangle}$ . This forms the second element  $\mathcal{O}_1$  of the basis.
- (4) The  $n$ th element of the Krylov basis is obtained by first evaluating

$$\mathcal{A}_n = [H, \mathcal{O}_{n-1}] - b_{n-1} \mathcal{O}_{n-2}.$$

- (5) This  $\mathcal{A}_n$  is orthonormal to all  $\mathcal{O}_k \forall k < n$ .
- (6) Finally, normalize  $\mathcal{A}_n$  to obtain  $\mathcal{O}_n = \frac{1}{b_n} \mathcal{A}_n$ . This is the  $n$ th Krylov vector.
- (7) Terminate this process at  $\mathcal{K}$  where  $b_{\mathcal{K}} = 0$  and  $b_{\mathcal{K}-1} > 0$ .

This is a version of the Lanczos algorithm [77]. The time-evolved operator  $\mathcal{O}(t)$  can now be written in the Krylov basis

$$\mathcal{O}(t) = e^{iHt} \mathcal{O}_0 e^{-iHt} = \sum_{n=0}^{\mathcal{K}} i^n \psi_n(t) \mathcal{O}_n. \quad (\text{A1})$$

The functions  $\psi_n(t)$  capture the time evolution of the operator  $\mathcal{O}$ . Note that this algorithm rewrites the Baker-Campbell-Hausdorff expansion of  $\mathcal{O}(t)$  in a more compact form by essentially orthonormalizing each term with respect to all the others. For the Hermitian initial operator (and Hamiltonian),  $i^k \mathcal{O}_k$  is also Hermitian.

The numbers  $b_n$  that have been collected from this algorithm uniquely fix all the functions  $\psi_n(t)$ . This is done by utilizing the fact that the autocorrelation function  $\psi_0(t) = \langle \mathcal{O}(t) | \mathcal{O}_0 \rangle$  can be expanded in a Taylor series [32,77] of the form

$$\psi_0(t) = \sum_k \frac{\mu_{2k}}{(2k)!} t^{2k}, \quad (\text{A2})$$

where  $b_1^2 b_2^2 \dots b_n^2 = \det(\mu_{i+j})_{0 \leq i, j \leq n}$ . Once the function  $\psi_0$  is known, the remaining  $\psi_k$  can be figured by using the recursion relation

$$\partial_t \psi_k(t) = -b_{k+1} \psi_{k+1}(t) + b_k \psi_{k-1}(t), \quad \psi_k(0) = \delta_{k0}, \quad (\text{A3})$$

which follows from applying Heisenberg's equation on  $\mathcal{O}(t)$ .

The sequence  $b_n$ , called the *Lanczos coefficients*, can be used to distinguish between chaotic and integrable dynamics in certain cases. The operator growth hypothesis [32] states that chaotic dynamics is characterized by an (asymptotic) linear growth of the Lanczos coefficients, i.e.,  $b_n \sim \alpha n$ . The average position of the operator can also be demonstrated on this basis

$$K(t) = \sum_n^{\kappa} n |\psi_n(t)|^2, \quad (\text{A4})$$

called the *Krylov complexity*, which grows (asymptotically) as  $K(t) \sim e^{2\alpha t}$  for chaotic systems. It is worth noting that this exponent also appears in the asymptotic decay rate of the spectral function  $\Phi(\omega) = \int_{-\infty}^{\infty} \psi_0(t) e^{i\omega t} dt$ :

$$\Phi(\omega \rightarrow \infty) \sim e^{-\pi|\omega|/2\alpha}. \quad (\text{A5})$$

The decay of the spectral function for large  $\omega$  has been the subject of intense investigation in recent years and has been found to be a useful indicator of chaotic and integrable dynamics [55,81,84–86].

A natural candidate for a Lyapunov exponent is the growth exponent  $\alpha$  of the Lanczos coefficients. For systems that demonstrate chaotic dynamics, it has been argued [32] that the autocorrelation function  $\psi_0(t)$  has poles on the imaginary axes, and the lowest-lying one is given by  $t_0 = \pm \frac{\pi}{2\alpha}$ . Therefore, the growth exponent  $\alpha$  can be extracted from the pole structure of the autocorrelation function.

In the systems that we study in the main text, we present the behavior of  $\alpha$  (rather, the behavior of the *Lyapunov time*  $T_\lambda = \alpha^{-1}$ ) by choosing an appropriate initial operator  $\mathcal{O}$  [87].

## APPENDIX B: CONSERVED QUANTITIES: SRN

When studying the SRN limit and computing the thermalization timescales, we choose the conserved quantity (in the integrable limit  $h \rightarrow 0$ ) to be the Pauli matrix  $\sigma_i^z$ , at some lattice site  $i$ . This quantity is local, and so the integrability breaking induces extra terms that are also local (but not necessarily 1–local). It is interesting to consider what would happen if a *nonlocal* conserved quantity is instead considered in the SRN case. The results do not change much for the following reasons: Let us consider the nonlocal initial operator

$$\mathcal{O}(N) = \sum_{i=1}^N \sigma_i^z, \quad (\text{B1})$$

where the superscript ( $N$ ) is used to indicate that the operator is nonlocal. Correspondingly, the local operator is denoted as  $\mathcal{O}^{(1)} = \sigma_1^z$ . The time evolution of the operator can be broken into that of individual  $\sigma_i^z$ . The evolutions for each of these should be equivalent since the state (with respect to which the expectation value is calculated)  $|\psi\rangle$  is a random state and hence has roughly equal weight at each site  $i$ . This allows us to approximate the fluctuation equation as

$$\langle \mathcal{O}^{(N)}(t) \rangle - \overline{\langle \mathcal{O}^{(N)} \rangle} \approx N(\langle \mathcal{O}^{(1)}(t) \rangle - \overline{\langle \mathcal{O}^{(1)} \rangle}), \quad (\text{B2})$$

which has a similar distribution of zeros and hence similar moments as that of  $\mathcal{O}^{(1)}$ .

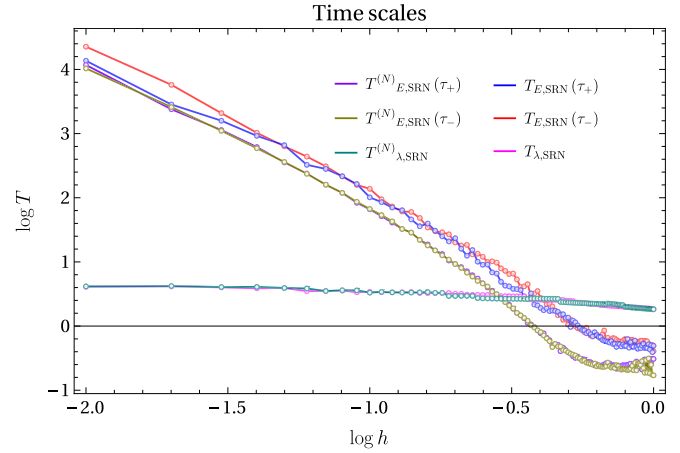


FIG. 4. Comparison of ergodization times and Lyapunov times for short-range network (SRN) with local and nonlocal operators. The superscript ( $N$ ) stands for the nonlocal operator. The initial states are different but chosen from the same random distribution, for the local and nonlocal cases.

The Krylov complexity (or Lanczos growth) of such nonlocal operators should also be the same as that of local operators. This is because we are working with translation symmetric systems, and therefore, each  $\sigma_i$  can be replaced by  $\sigma_1$  in the BCH expansion. The resulting overall factor of  $N$  is taken care of via normalization.

To support this argument, we present the numerical results for the two cases in Fig. 4. The nonlocal timescales are represented by a superscript ( $N$ ).

It is interesting to note that the ergodization timescales for  $\tau_{\pm}$  are much more similar for the case of  $\mathcal{O}^{(N)}$  than for  $\mathcal{O}^{(1)}$ . This is due to the sum of local operators having a smoothing effect on the random state  $|\psi\rangle$ . This causes the timescales obtained from  $\tau_+$  and  $\tau_-$  to almost exactly overlap in the weakly integrable limit.

## APPENDIX C: CONSERVED QUANTITIES: LRN

Here, we discuss the conserved quantities of the integrable limit  $g \rightarrow 0$  of the LRN class. This integrable Hamiltonian is known as the TFIM and has a complete set of conserved quantities. These are given by

$$I^{(k)} = iJ \sum_{j=1}^N (S_{j:j+k}^{zy} - S_{j:j+k}^{yz}), \quad k = 1, \dots, N-1, \quad (\text{C1})$$

where we have the following shorthand

$$S_{j:j+l}^{\alpha\beta} = \sigma_j^\alpha \left( \prod_{n=1}^{l-1} \sigma_{j+n}^x \right) \sigma_{j+l}^\beta. \quad (\text{C2})$$

It is straightforward to see that  $[H_{\text{TFIM}}, I^{(k)}] = 0$ . These quantities can be interpreted as linear combinations of mode occupation numbers in the Jordan-Wigner fermion theory [88]. For  $k = N$ , the conserved quantity corresponds to  $\prod_{i=1}^N \sigma_i^x$ , which is a symmetry operation corresponding to the replacement  $\sigma^{z,y} \rightarrow -\sigma^{z,y}$ .

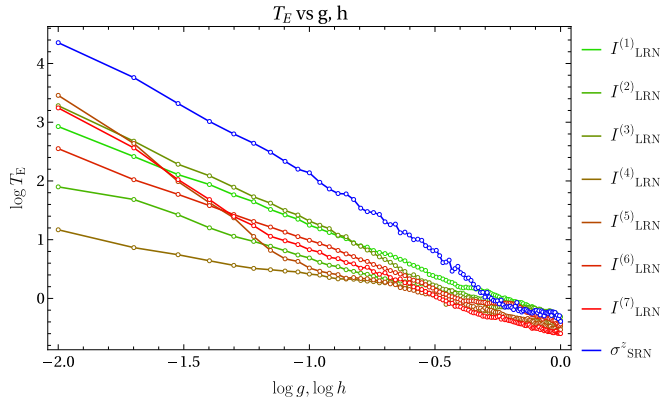


FIG. 5. Scaling of ergodization times for long-range network [LRN; for all conserved quantities  $I^{(k)}$ ] and comparison with the same for short-range network (SRN; single operator).

We compare the ergodization times  $T_{E,\pm}$  for each  $I_k$ , with the respective Lyapunov time  $T_\lambda$  obtained via the Krylov method. The results are presented in Fig. 5. It is evident that the scaling is different for different  $I^{(k)}$ . Note that, despite different scaling behavior of the ergodization time  $T_E$  for different conserved quantities  $I^{(k)}$ , the ergodization time for the  $\sigma^z$  operator in the SRN case bounds the  $T_E$  for all  $I^{(k)}$  from above. Assuming a power-law scaling behavior for the timescales

$$\log T_{E,\lambda} = \begin{cases} \alpha_{E,\lambda} \log g + \delta_{E,\lambda}, & \text{LRN,} \\ \alpha_{E,\lambda} \log h + \delta_{E,\lambda}, & \text{SRN,} \end{cases} \quad (\text{C3})$$

we obtain the exponents listed in Table I.

For the corresponding SRN case, we observe that the coefficients are

$$\begin{aligned} \alpha_{E,\text{SRN}}^+ &= -2.26301, & \delta_{E,\text{SRN}}^+ &= -0.136552, \\ \alpha_{\lambda,\text{SRN}} &= -0.0817788, & \delta_{\lambda,\text{SRN}} &= 0.217633. \end{aligned}$$

It is also instructive to compare the scaling of the ratio of timescales  $T_E/T_\lambda$  as a function of  $T_\lambda$ . This ratio is expected to diverge upon approaching the integrable limit (i.e., as  $T_\lambda$  increases). Since different conserved quantities will, in general, have different ranges of values of  $T_\lambda$  (although within the same order), it is better to instead study the ratio as a function of  $T_\lambda/\max(T_\lambda)$ . We present this result in Fig. 6.

TABLE I. Power-law coefficients for all  $I^{(k)}$  for the LRN case. The superscript + stands for results extracted from positive passage times. The results for negative passage times are comparable.

$k$	$\alpha_E^+$	$\delta_E^+$	$\alpha_\lambda$	$\delta_\lambda$
1	-1.65828	-0.395546	-0.046659	0.262234
2	-1.28645	-0.592328	-0.0204276	0.248453
3	-1.9492	-0.638931	-0.151105	0.00884637
4	-0.734752	-0.356261	-0.169417	-0.0685405
5	-3.03973	-2.60729	-0.154005	-0.0406314
6	-1.54398	-0.570509	-0.155603	-0.0419308
7	-2.49685	-1.76273	-0.196703	-0.11035

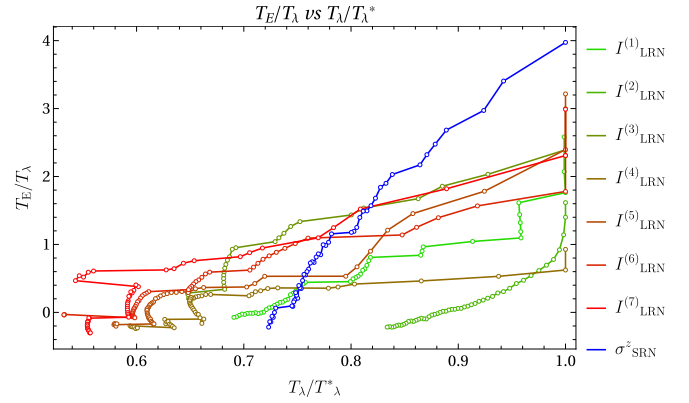


FIG. 6. Behavior of the ratio  $T_E/T_\lambda$  as a function of  $T_\lambda/T_\lambda^*$ , where  $T_\lambda^* = \max(T_\lambda)$ . The scaling for all  $I^{(k)}$  [long-range network (LRN)] is compared with that of  $\sigma^z$  [short-range network (SRN)]. These results are presented for the integrability-breaking parameter  $\sim 0$ .

Finally, we consider the scaling of  $T_\lambda$  and  $T_E/T_\lambda$  with the integrability-breaking parameter  $g, h$  for completeness. This is presented in Figs. 7 and 8, respectively. The results of Figs. 7 and 5 explain the observation in Fig. 8 since the Lyapunov times  $T_\lambda$  for all  $I^{(k)}$  (LRN) and  $\sigma^z$  (SRN) remain comparable throughout the range of  $g, h$  explored. However, the ergodization times scale in a different manner (significantly different, on the log-scale, as seen in Fig. 5). Thus, the ratio  $T_E/T_\lambda$  is also highly sensitive to initial operator choice and the universality classification.

#### APPENDIX D: PASSAGE TIMES

The expectation value of an operator  $mop$  oscillates around its mean value at long times. Consider a Hamiltonian  $H$  and some operator  $\mathcal{O}$  whose time evolution is studied under this Hamiltonian. This is schematically shown in the Fig. 9. The time-evolved operator is given by

$$\mathcal{O}(t) = e^{-iHt} \mathcal{O}(t) e^{iHt}. \quad (\text{D1})$$

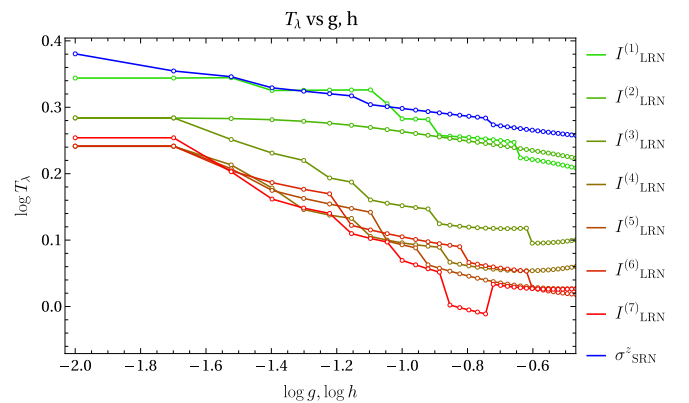


FIG. 7. Behavior of the Lyapunov times  $T_\lambda$  as a function of the integrability-breaking parameter  $g, h$ . The region close to the integrable limit is explored. It is observed that, for all conserved quantities  $I^{(k)}$  [long-range network (LRN)] as well as for the short-range network (SRN) observable  $\sigma^z$ , the Lyapunov times are comparable.

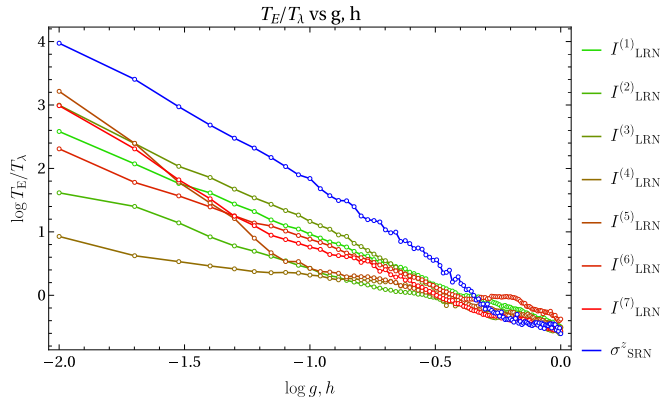


FIG. 8. Behavior of the ratio  $T_E/T_\lambda$  as a function of the integrability-breaking parameter  $g, h$ . The results support the conclusion of Fig. 5.

The expectation value of this operator in a generic state  $|\psi\rangle$  is given by

$$\langle \mathcal{O}(t) \rangle = \langle \psi | e^{-iHt} \mathcal{O} e^{iHt} | \psi \rangle. \quad (\text{D2})$$

The generic state is written as follows in terms of the eigenstates  $|n\rangle$  of the Hamiltonian  $H$ :

$$|\psi\rangle = \sum_n c_n |n\rangle. \quad (\text{D3})$$

The expectation value  $\langle \mathcal{O}(t) \rangle$  can now be rewritten as

$$\langle \mathcal{O}(t) \rangle = \sum_{m,n} c_n c_m^* \exp[i(E_n - E_m)t] \langle m | \mathcal{O} | n \rangle. \quad (\text{D4})$$

The time-averaged value of this expectation is given as

$$\bar{\mathcal{O}} = \lim_{T \rightarrow \infty} \frac{1}{T} \int_0^T \langle \mathcal{O}(t) \rangle dt \quad (\text{D5})$$

$$= \lim_{T \rightarrow \infty} \sum_{m,n} c_n c_m^* \langle m | \mathcal{O} | n \rangle \left\{ \frac{1}{T} \int_0^T \exp[i(E_n - E_m)t] dt \right\}. \quad (\text{D6})$$

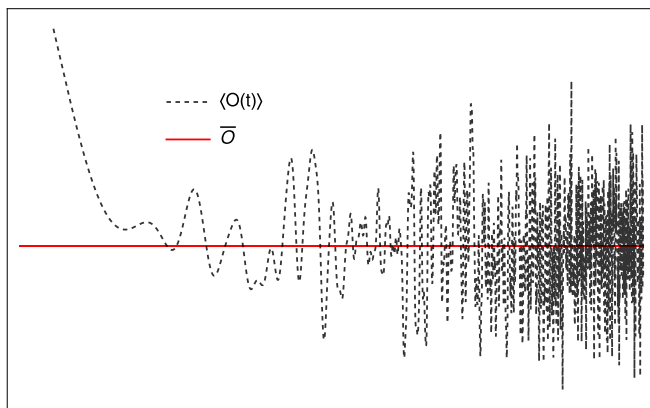


FIG. 9. Schematic representation of time-evolution of  $\langle \mathcal{O}(t) \rangle$  around the mean value  $\bar{\mathcal{O}}$ . We have used a log scale on the  $t$  axis.

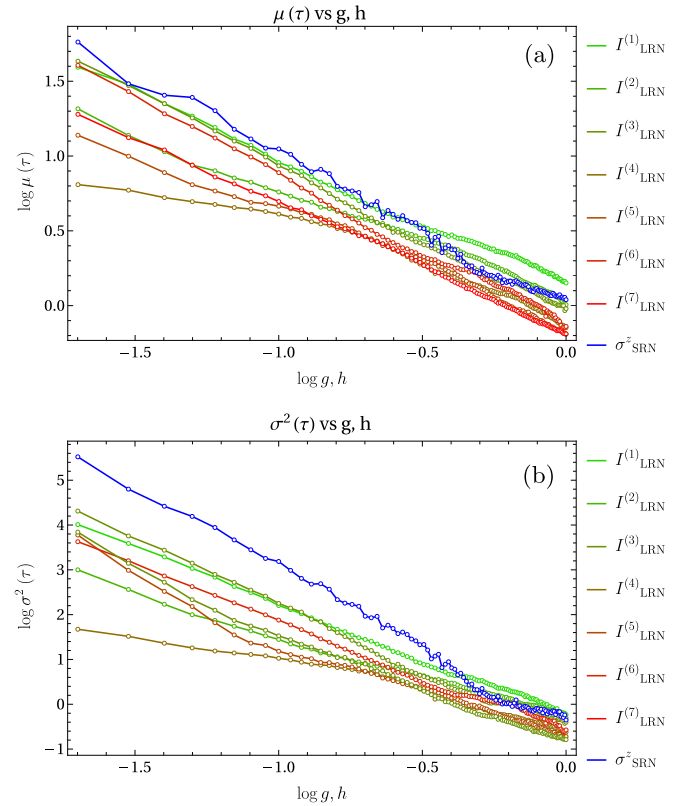


FIG. 10. Mean and variance of ergodization times for all operators  $I^{(k)}$  and the short-range network (SRN) operator  $\sigma^z$ , as a function of  $g$  and  $h$ , respectively. (a) Mean of ergodization times  $\mu(\tau)$  and (b) Variance of ergodization times  $\sigma^2(\tau)$ .

The integral over  $t$  gives  $\delta(E_n - E_m)$ . Therefore, the final result is

$$\bar{\mathcal{O}} = \sum_n |c_n|^2 \langle n | \mathcal{O} | n \rangle + \sum_{n', m'} c_n c_m^* \langle m' | \mathcal{O} | n' \rangle, \quad (\text{D7})$$

where the second sum is over all  $n', m'$  for which  $E(n') = E(m')$ . Thus, if the mean value is subtracted from  $\langle \mathcal{O}(t) \rangle$ , we obtain

$$\begin{aligned} f_{\mathcal{O}}(t) &= \langle \mathcal{O}(t) \rangle - \bar{\mathcal{O}} \\ &= \sum_{m, n - \{m', n'\}} c_n c_m^* \exp[i(E_n - E_m)t] \langle m | \mathcal{O} | n \rangle \\ &\quad - \sum_n |c_n|^2 \langle n | \mathcal{O} | n \rangle, \end{aligned} \quad (\text{D8})$$

where the terms corresponding to degeneracies were dropped. This captures the behavior of the off-diagonal elements of the time-evolved operator.

We evaluate the distribution of the zeros of the function  $f_{\mathcal{O}}(t)$  and determine how they are spaced. The moments of the distribution of this spacing can be interpreted as another natural timescale. Note that, for random uniform initial state (i.e.,  $c_n$  are uniform random numbers), this distribution is determined by the level spacing distribution of the Hamiltonian and the off-diagonal elements of the initial operator [89].

The passage or excursion times are then defined as the interval  $\tau_i$  between the zeros  $t_i$  and  $t_{i+1}$  of the function  $f_{\mathcal{O}}(t)$ .

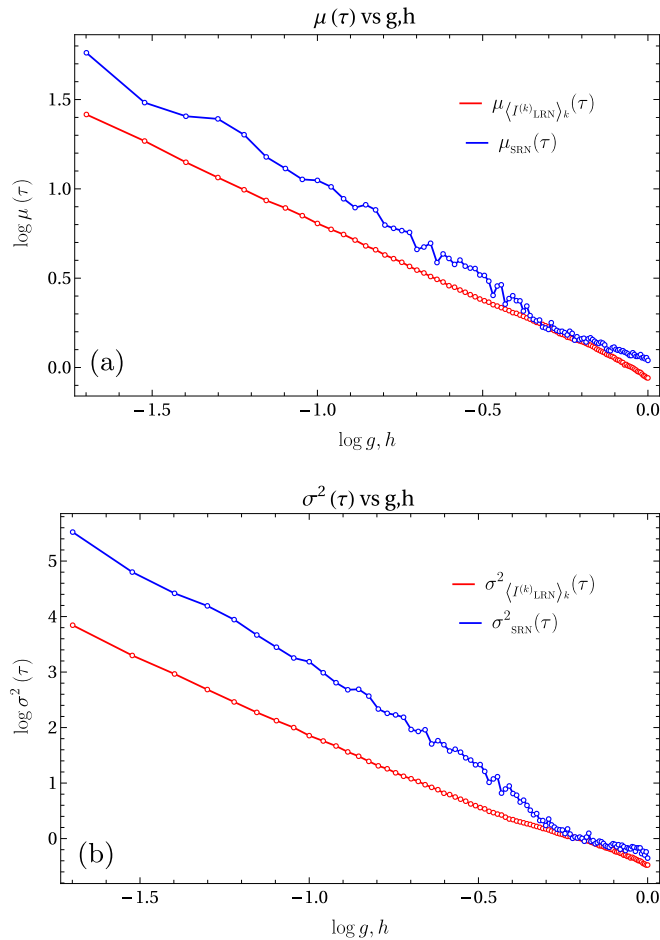


FIG. 11. Mean and variance of ergodization times for the averaged operator  $N^{-1} \sum_k I^{(k)}$  and the short-range network (SRN) operator  $\sigma^2$ , as a function of  $g$  and  $h$ , respectively. (a) Mean of ergodization times  $\mu(\tau)$  and (b) Variance of ergodization times  $\sigma^2(\tau)$ .

There are two passage times which are extracted from this information. The first is the positive passage time  $\tau_{i,+}$  which corresponds to  $f_{\mathcal{O}}(t)$  being positive in the interval  $t_i$  to  $t_{i+1}$ . The negative passage time  $\tau_{j,-}$  corresponds to  $f_{\mathcal{O}}(t)$  being negative in the interval  $t_j$  to  $t_{j+1}$ . In this paper, we study the statistical distribution of  $\tau_{i,\pm}$  through their mean and variance (and combinations thereof).

## APPENDIX E: DETAILS OF THE NUMERICS

In this section, we discuss the details of the numerical computations and present some of the results that are mentioned in the main text.

While determining the passage times, our approach involved first diagonalizing the Hamiltonian  $H$  in Eq. (1) to find its eigenvalues and eigenvectors. The next step is determining the coefficients  $c_n$  corresponding to the initial state  $\psi$ , drawn from a uniform distribution, and the components of the initial operator  $\langle m|\mathcal{O}|n\rangle$  and then plugging it into the expression in Eq. (D8). Then this function was evaluated numerically by varying  $t$  in steps of  $t_0 = \min_{m \neq n} \frac{1}{4(E_m - E_n)}$  and the values  $t = t_i$  for which  $f(t_i) = 0$  were collected. Finally, the difference  $\tau_i = t_{i+1} - t_i$  was computed to determine the excursion times. We collected  $\sim 10^4$  passages.

The results for the SRNs and LRNs are discussed in the main text. For the SRNs and LRNs, the appropriate choice of ergodization time is the ratio of variance and mean of the excursion times as supported by the data shown in Figs. 10 and 11. The exponentially larger scale of  $\sigma^2$  than  $\mu$  suggests that the fluctuations dominate the dynamics. Therefore, the appropriate choice of a timescale would be a ratio of the fluctuation to the mean, given by  $\frac{\sigma^2}{\mu}$ . This is found to be the case in both LRN and SRN.

- [1] O. Bohigas, M. J. Giannoni, and C. Schmit, Characterization of chaotic quantum spectra and universality of level fluctuation laws, *Phys. Rev. Lett.* **52**, 1 (1984).
- [2] M. V. Berry, M. Tabor, and J. M. Ziman, Level clustering in the regular spectrum, *Proc. R. Soc. Lond. A* **356**, 375 (1977).
- [3] J. Zakrzewski, Quantum chaos and level dynamics, *Entropy* **25**, 491 (2023).
- [4] F. Haake, *Quantum Signatures of Chaos* (Springer-Verlag, Berlin, 2006).
- [5] E. Brézin and S. Hikami, Spectral form factor in a random matrix theory, *Phys. Rev. E* **55**, 4067 (1997).
- [6] A. M. García-García and J. J. M. Verbaarschot, Spectral and thermodynamic properties of the Sachdev-Ye-Kitaev model, *Phys. Rev. D* **94**, 126010 (2016).
- [7] A. M. García-García and J. J. M. Verbaarschot, Analytical spectral density of the Sachdev-Ye-Kitaev model at finite N, *Phys. Rev. D* **96**, 066012 (2017).
- [8] M. Khrantsov and E. Lanina, Spectral form factor in the double-scaled SYK model, *J. High Energy Phys.* **03** (2021) 031.
- [9] P. J. Forrester, *Log-Gases and Random Matrices (LMS-34)* (Princeton University Press, Princeton, 2010).
- [10] M. L. Mehta, *Random Matrices*, 3rd ed. (Elsevier/Academic Press, Amsterdam, 2004).
- [11] D. Stanford, Many-body chaos at weak coupling, *J. High Energy Phys.* **11** (2016) 009.
- [12] P. Caputa, T. Numasawa, and A. Veliz-Orsorio, Out-of-time-ordered correlators and purity in rational conformal field theories, *PTEP* **2016**, 113B06 (2016).
- [13] D. A. Roberts and B. Yoshida, Chaos and complexity by design, *J. High Energy Phys.* **04** (2017) 121.
- [14] H. Shen, P. Zhang, R. Fan, and H. Zhai, Out-of-time-order correlation at a quantum phase transition, *Phys. Rev. B* **96**, 054503 (2017).
- [15] J. Cotler, N. Hunter-Jones, J. Liu, and B. Yoshida, Chaos, complexity, and random matrices, *J. High Energy Phys.* **11** (2017) 048.
- [16] J. S. Cotler, D. Ding, and G. R. Penington, Out-of-time-order operators and the butterfly effect, *Ann. Phys.* **396**, 318 (2018).
- [17] K. Hashimoto, K. Murata, and R. Yoshii, Out-of-time-order correlators in quantum mechanics, *J. High Energy Phys.* **10** (2017) 138.

- [18] R. Fan, P. Zhang, H. Shen, and H. Zhai, Out-of-time-order correlation for many-body localization, *Sci. Bull.* **62**, 707 (2017).
- [19] Z.-H. Sun, J.-Q. Cai, Q.-C. Tang, Y. Hu, and H. Fan, Out-of-time-order correlators and quantum phase transitions in the Rabi and Dicke models, *Ann. Phys.* **532**, 1900270 (2020).
- [20] N. Tsuji, T. Shitara, and M. Ueda, Out-of-time-order fluctuation-dissipation theorem, *Phys. Rev. E* **97**, 012101 (2018).
- [21] R. de Mello Koch, J.-H. Huang, C.-T. Ma, and H. J. R. Van Zyl, Spectral form factor as an OTOC averaged over the Heisenberg group, *Phys. Lett. B* **795**, 183 (2019).
- [22] T. Akutagawa, K. Hashimoto, T. Sasaki, and R. Watanabe, Out-of-time-order correlator in coupled harmonic oscillators, *J. High Energy Phys.* **08** (2020) 013.
- [23] J. Hu and S. Wan, Out-of-time-ordered correlation in the anisotropic Dicke model, *Commun. Theor. Phys.* **73**, 125703 (2021).
- [24] J. Haferkamp, P. Faist, N. B. T. Kothakonda, J. Eisert, and N. Y. Halpern, Linear growth of quantum circuit complexity, *Nat. Phys.* **18**, 528 (2022).
- [25] J. M. Magán, Black holes, complexity and quantum chaos, *J. High Energy Phys.* **09** (2018) 043.
- [26] S. Chapman and G. Policastro, Quantum computational complexity from quantum information to black holes and back, *Eur. Phys. J. C* **82**, 128 (2022).
- [27] S. Roca-Jerat, T. Sancho-Lorente, J. Román-Roche, and D. Zueco, Circuit complexity through phase transitions: Consequences in quantum state preparation, *SciPost Phys.* **15**, 186 (2023).
- [28] P. Zhang and Z. Yu, Dynamical transition of operator size growth in quantum systems embedded in an environment, *Phys. Rev. Lett.* **130**, 250401 (2023).
- [29] L. Agarwal and S. Xu, Emergent symmetry in Brownian SYK models and charge dependent scrambling, *J. High Energy Phys.* **02** (2022) 045.
- [30] D. A. Roberts, D. Stanford, and A. Streicher, Operator growth in the SYK model, *J. High Energy Phys.* **06** (2018) 122.
- [31] T. Zhou and X. Chen, Operator dynamics in a Brownian quantum circuit, *Phys. Rev. E* **99**, 052212 (2019).
- [32] D. E. Parker, X. Cao, A. Avdoshkin, T. Scaffidi, and E. Altman, A universal operator growth hypothesis, *Phys. Rev. X* **9**, 041017 (2019).
- [33] J. L. F. Barbón, E. Rabinovici, R. Shir, and R. Sinha, On the evolution of operator complexity beyond scrambling, *J. High Energy Phys.* **10** (2019) 264.
- [34] E. Rabinovici, A. Sánchez-Garrido, R. Shir, and J. Sonner, Operator complexity: A journey to the edge of Krylov space, *J. High Energy Phys.* **62** (2021) 1029.
- [35] E. Rabinovici, A. Sánchez-Garrido, R. Shir, and J. Sonner, Krylov complexity from integrability to chaos, *J. High Energy Phys.* **07** (2022) 151.
- [36] E. Rabinovici, A. Sánchez-Garrido, R. Shir, and J. Sonner, Krylov localization and suppression of complexity, *J. High Energy Phys.* **03** (2022) 211.
- [37] B. Bhattacharjee, X. Cao, P. Nandy, and T. Pathak, Krylov complexity in saddle-dominated scrambling, *J. High Energy Phys.* **05** (2022) 174.
- [38] B. Bhattacharjee, S. Sur, and P. Nandy, Probing quantum scars and weak ergodicity breaking through quantum complexity, *Phys. Rev. B* **106**, 205150 (2022).
- [39] B. Bhattacharjee, A Lanczos approach to the adiabatic gauge potential, [arXiv:2302.07228](https://arxiv.org/abs/2302.07228).
- [40] M. Malishava, Thermalization of classical weakly nonintegrable many-body systems, [arXiv:2211.01887](https://arxiv.org/abs/2211.01887).
- [41] M. Malishava and S. Flach, Lyapunov spectrum scaling for classical many-body dynamics close to integrability, *Phys. Rev. Lett.* **128**, 134102 (2022).
- [42] G. M. Lando and S. Flach, Thermalization slowing down in multidimensional Josephson junction networks, *Phys. Rev. E* **108**, L062301 (2023).
- [43] W. Zhang, G. M. Lando, B. Dietz, and S. Flach, Thermalization universality-class transition induced by Anderson localization, *Phys. Rev. Res.* **6**, L012064 (2024).
- [44] C. Danieli, D. K. Campbell, and S. Flach, Intermittent many-body dynamics at equilibrium, *Phys. Rev. E* **95**, 060202(R) (2017).
- [45] C. Danieli, T. Mithun, Y. Kati, D. K. Campbell, and S. Flach, Dynamical glass in weakly nonintegrable Klein-Gordon chains, *Phys. Rev. E* **100**, 032217 (2019).
- [46] T. Mithun, Y. Kati, C. Danieli, and S. Flach, Weakly nonergodic dynamics in the Gross-Pitaevskii lattice, *Phys. Rev. Lett.* **120**, 184101 (2018).
- [47] T. Mithun, C. Danieli, Y. Kati, and S. Flach, Dynamical glass and ergodization times in classical Josephson junction chains, *Phys. Rev. Lett.* **122**, 054102 (2019).
- [48] G. Bel and E. Barkai, Weak ergodicity breaking in the continuous-time random walk, *Phys. Rev. Lett.* **94**, 240602 (2005).
- [49] M. Rigol, Breakdown of thermalization in finite one-dimensional systems, *Phys. Rev. Lett.* **103**, 100403 (2009).
- [50] M. Srednicki, Chaos and quantum thermalization, *Phys. Rev. E* **50**, 888 (1994).
- [51] J. M. Deutsch, Quantum statistical mechanics in a closed system, *Phys. Rev. A* **43**, 2046 (1991).
- [52] L. D'Alessio, Y. Kafri, A. Polkovnikov, and M. Rigol, From quantum chaos and eigenstate thermalization to statistical mechanics and thermodynamics, *Adv. Phys.* **65**, 239 (2016).
- [53] J. M. Magan, Random free fermions: An analytical example of eigenstate thermalization, *Phys. Rev. Lett.* **116**, 030401 (2016).
- [54] J. M. Deutsch, Eigenstate thermalization hypothesis, *Rep. Prog. Phys.* **81**, 082001 (2018).
- [55] M. Brenes, T. LeBlond, J. Goold, and M. Rigol, Eigenstate thermalization in a locally perturbed integrable system, *Phys. Rev. Lett.* **125**, 070605 (2020).
- [56] D. L. Jafferis, D. K. Kolchmeyer, B. Mukhametzhanov, and J. Sonner, Matrix models for eigenstate thermalization, [arXiv:2209.02130](https://arxiv.org/abs/2209.02130).
- [57] J. Wang, M. H. Lamann, J. Richter, R. Steinigeweg, A. Dymarsky, and J. Gemmer, Eigenstate thermalization hypothesis and its deviations from random-matrix theory beyond the thermalization time, *Phys. Rev. Lett.* **128**, 180601 (2022).
- [58] A. Dymarsky, Bound on eigenstate thermalization from transport, *Phys. Rev. Lett.* **128**, 190601 (2022).
- [59] T. L. M. Lezama, E. J. Torres-Herrera, F. Pérez-Bernal, Y. Bar Lev, and L. F. Santos, Equilibration time in many-body quantum systems, *Phys. Rev. B* **104**, 085117 (2021).
- [60] M. Schiulaz, A. Silva, and M. Müller, Dynamics in many-body localized quantum systems without disorder, *Phys. Rev. B* **91**, 184202 (2015).

- [61] E. B. Rozenbaum, S. Ganeshan, and V. Galitski, Lyapunov exponent and out-of-time-ordered correlator's growth rate in a chaotic system, *Phys. Rev. Lett.* **118**, 086801 (2017).
- [62] A. Hallam, J. G. Morley, and A. G. Green, The Lyapunov spectra of quantum thermalisation, *Nat. Commun.* **10**, 2708 (2019).
- [63] H. Gharibyan, M. Hanada, B. Swingle, and M. Tezuka, Quantum Lyapunov spectrum, *J. High Energy Phys.* **04** (2019) 082.
- [64] A. Chan, A. De Luca, and J. T. Chalker, Spectral Lyapunov exponents in chaotic and localized many-body quantum systems, *Phys. Rev. Res.* **3**, 023118 (2021).
- [65] J. Maldacena, S. H. Shenker, and D. Stanford, A bound on chaos, *J. High Energy Phys.* **08** (2016) 106.
- [66] P. Pfeuty, The one-dimensional Ising model with a transverse field, *Ann. Phys.* **57**, 79 (1970).
- [67] S. Sachdev, *Handbook of Magnetism and Advanced Magnetic Materials* (John Wiley and Sons, Ltd, New York, 2007).
- [68] M. C. Bañuls, J. I. Cirac, and M. B. Hastings, Strong and weak thermalization of infinite nonintegrable quantum systems, *Phys. Rev. Lett.* **106**, 050405 (2011).
- [69] D. A. Roberts, D. Stanford, and L. Susskind, Localized shocks, *J. High Energy Phys.* **03** (2015) 051.
- [70] A. Lakshminarayan and V. Subrahmanyam, Multipartite entanglement in a one-dimensional time-dependent Ising model, *Phys. Rev. A* **71**, 062334 (2005).
- [71] C.-J. Lin and O. I. Motrunich, Out-of-time-ordered correlators in a quantum Ising chain, *Phys. Rev. B* **97**, 144304 (2018).
- [72] B. Craps, M. De Clerck, D. Janssens, V. Luyten, and C. Rabideau, Lyapunov growth in quantum spin chains, *Phys. Rev. B* **101**, 174313 (2020).
- [73] Nivedita, H. Shackleton, and S. Sachdev, Spectral form factors of clean and random quantum Ising chains, *Phys. Rev. E* **101**, 042136 (2020).
- [74] Corresponding to the fermionic operators in the Jordan-Wigner representation of the system.
- [75] Somewhat related to this is the delocalization in Fock space, which has been studied in Ref. [90].
- [76] Minimal with respect to a cost function, which in this case is the Krylov complexity itself.
- [77] V. Viswanath and G. Müller, *The Recursion Method: Application to Many Body Dynamics*, Lecture Notes in Physics Monographs (Springer, Berlin, 1994).
- [78] Y. Zhang, L. Vidmar, and M. Rigol, Statistical properties of the off-diagonal matrix elements of observables in eigenstates of integrable systems, *Phys. Rev. E* **106**, 014132 (2022).
- [79] J. Richter, A. Dymarsky, R. Steinigeweg, and J. Gemmer, Eigenstate thermalization hypothesis beyond standard indicators: Emergence of random-matrix behavior at small frequencies, *Phys. Rev. E* **102**, 042127 (2020).
- [80] F. Fritzsche and T. Prosen, Eigenstate thermalization in dual-unitary quantum circuits: Asymptotics of spectral functions, *Phys. Rev. E* **103**, 062133 (2021).
- [81] L. Vidmar, B. Krajewski, J. Bonča, and M. Mierzejewski, Phenomenology of spectral functions in disordered spin chains at infinite temperature, *Phys. Rev. Lett.* **127**, 230603 (2021).
- [82] Other forms of comparison have the underlying assumption that the integrability-breaking parameters  $g$  and  $h$  can be treated similarly. Comparison of  $T_{E,\pm}/T_\lambda$  with  $T_\lambda/T_\lambda^*$  frees us of this assumption.
- [83] J. Karthik, A. Sharma, and A. Lakshminarayan, Entanglement, avoided crossings, and quantum chaos in an Ising model with a tilted magnetic field, *Phys. Rev. A* **75**, 022304 (2007).
- [84] T. LeBlond, D. Sels, A. Polkovnikov, and M. Rigol, Universality in the onset of quantum chaos in many-body systems, *Phys. Rev. B* **104**, L201117 (2021).
- [85] T. LeBlond, K. Mallayya, L. Vidmar, and M. Rigol, Entanglement and matrix elements of observables in interacting integrable systems, *Phys. Rev. E* **100**, 062134 (2019).
- [86] M. Brenes, J. Goold, and M. Rigol, Low-frequency behavior of off-diagonal matrix elements in the integrable XXZ chain and in a locally perturbed quantum-chaotic XXZ chain, *Phys. Rev. B* **102**, 075127 (2020).
- [87] A more accurate notion of the Lyapunov time would be to define it as the time at which the Krylov complexity becomes of the order of  $\mathcal{K}$  (let us call it  $\tau_*$ ). Here,  $\mathcal{K}$  is the saturation value of Krylov complexity. It is related to the dimension of the Krylov space (usually much less than that). The difference between the two choices is a factor of  $O(1)$  in the systems we study. Thus, the ratio between  $\tau_*$  and  $T_\lambda = \alpha^{-1}$  turns out to be  $O(1)$ . Hence, the study of  $\alpha^{-1}$  is sufficient.
- [88] M. Fagotti and F. H. L. Essler, Reduced density matrix after a quantum quench, *Phys. Rev. B* **87**, 245107 (2013).
- [89] Corresponding to the off-diagonal fluctuation in ETH.
- [90] V. B. Bulchandani, D. A. Huse, and S. Gopalakrishnan, Onset of many-body quantum chaos due to breaking integrability, *Phys. Rev. B* **105**, 214308 (2022).